Alexander Stadnik
Senior Lecturer
Donbass State Engineering Academy
Department of fundamentals
of machine design
Ukraine

Sergii Podlesny
Associate professor
Donbass State Engineering Academy
Department of fundamentals
of machine design
Ukraine

Svitlana Kaporovych
Senior Lecturer
Donbass State Engineering Academy
Department of fundamentals
of machine design
Ukraine

Oleksii Kabatskyi
Associate professor
Donbass State Engineering Academy
Department of fundamentals
of machine design
Ukraine

Spatial Transportation of The Beam on a Bifilar Fastening

The complex problem of the spatial motion of the "trolley-beam" mechanical system is investigated. Three stages are considered: 1) movement of the beam on a bifilar suspension to the movable trolley; 2) movement of the beam after the breakage of one branch of the suspension; 3) movement of the beam after the breakage of the second branch of the suspension. The study was carried out by creating mathematical models for each stage of the system movement and then conducting a numerical experiment using computer algebra. The tension of the ropes is calculated at the first and second stages of the system movement. Their extreme values are determined. The obtained results will be used in the further study of the system to reduce the tension of the rope and oscillation amplitude and to prevent accidents.

Keywords: *cargo transportation, bifilar fastening, DOF model, Lagrange equation, numerical simulation, rope tension, breakage.*

1. INTRODUCTION

Lifting and transport machines and mechanisms are widely used in industry, construction, and transport for lifting, moving, and unloading heavy loads with distributed mass. The main types of these machines include gantry, overhead, and tower cranes.

Due to the influence of internal and external force factors, the load's uncontrolled pendulum spatial oscil–lations (swings) usually occur. They significantly redu–ce the productivity and accuracy of the work performed.

The problem of ensuring the safe and high-per–formance operation of cranes is urgent. Due to reducing the time of damping the load oscillations, its solution will significantly increase the accuracy of working out the specified trajectories of the load movement in space and the productivity of lifting and transport, const–ruction, and installation work.

It's impossible to develop and improve cranes in the future without studying loads and their impact on stability under various operating conditions.

Based on the requirements for crane design and control, researchers are trying to understand the crane system dynamics' physical nature and engineering implications, including payloads [1-6]. In connection with those mentioned above, studying the behavior of complex pendulum systems for moving heavy loads with distributed mass by crane is an urgent task.

2. LITERATURE REVIEW AND PROBLEM STATE–MENT

A very simplified model for moving a point load by a trolley of an overhead crane is the elliptical pendulum model used in works [7-16].

A more advanced one is the flat model of a double pendulum suspended from a horizontally moving trolley, such as a gantry or an overhead crane [17-20]. However, to get closer to real practical problems, flat models should be replaced with spatial ones (2D models should be replaced with 3D models).

In a number of works, a model of a spherical pen–dulum with a movable suspension point is considered a 3D model for cargo movement by a crane, taking into account the elastic properties of the rope and the action of an external wind load [21-33].

The 3D models of the double spherical 3D pen–dulum studied in the works [34-37] are more advanced. However, loads of point mass, not of distributed mass, are considered in these works.

The study of the movement of loads with distributed mass, for example, in the form of a beam, is of much greater interest. Such problems in flat design are considered in works [38-41].

Spatial 3D models of the movement of loads in the form of a beam were studied in works [42-44]. In addition, almost nowhere the rope tension during movement or at the time of a possible break was determined. At the same time, it is possible to use other options for fastening the load (beams), choose other coordinate systems, and use other theorems and principles for simulating and studying the dynamics of a mechanical system.

There is a study of a flat (not spatial) model of the beam behavior after the breakage of one of the rope branches of the overhead crane [45].

The research examines the dynamics of the mechanical system "distributed mass load with a bifilar fastening to the trolley." the analysis of references shows the dynamics of loads transportation by an overhead crane with a bifilar beam fastening are not fully considered in the available works. In the proposed

Received: May 2022, Accepted: August 2022
Correspondence to: Ph.D. Svitlana Kaporovych,
Donbass State Engineering Academy,
72 Akademicheskaya STR., Kramatorsk, Ukraine
E-mail: kaporovych@gmail.com
doi:10.5937/fme2203548S

formulation, the task was not previously considered. Calculating the rope tension during the movement of the load is of particular interest for considering emergencies associated with the break of the rope (fastening) and simulating the subsequent behavior of the load. This confirms the relevance and industrial significance of this study.

3. THE PURPOSE AND OBJECTIVES OF THE STUDY

The purpose of this research is a dynamic description of the complex problem of spatial movement of a mechanical system in three stages. In the first stage, the movement of the system "a trolley with the beam *AB* bifilar fastening" is considered (Fig. 1). A 4-DOF mechanical system is studied, where *AB=DE* and *AE=BD*. In the second stage, movement of this system in the event of the breakage of one of the ropes is considered. In the third stage, the beam's spatial movement after the second rope's breakage is investigated. The purpose is also to determine the tension of the ropes, simulate possible emergencies associated with the breakage of the ropes, and study the further movement of the load.

The subject of this research is to study oscillations of the beam *AB* and the trolley *DE* at the first and second stages, to determine the change in the rope tension over time, calculate the extreme tension values, and study the beam movement at the third stage.

The main novelty of this study lies in the deve–lopment of a new mathematical 4-DOF model of the mechanical system "trolley – beam on a bifilar fas–tening" with further dynamic analysis of the system oscillations and numerical estimation of the rope tension at the first stage, study of the 5-DOF model of the mec–hanical system "trolley - rope - beam" and deter–mination of the rope tension at the second stage as well as simulation of the beam *AB* spatial motion with the usage of the 5-DOF model at the third stage. All three models are related. The final conditions of the previous stage are the initial conditions of the next stage.

4. MATERIALS AND METHODS

4.1 Kinematics of a mechanical system. Geometric constraints. Coordinates and speeds

The mechanical 4-DOF model is shown in Figure 1.

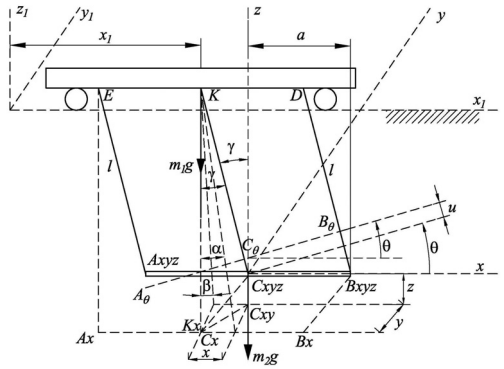

Figure 1. Computational scheme for the transportation of the beam *AB* by traverse *DE* with the usage of bifilar fastening

The dynamic equations for the motion of the mechanical system will be obtained by using Lagrange equations of the second kind.

Figure 1 shows the following parameters of the mechanical system: g = 9.81 (m/s^2) – acceleration of gravity; m_1 – the mass of the crane with the traverse *ED,* moving forward, m_2 – the mass of the beam *AB*; l – the length of the ropes *AE* and *BD*; $2a$ – the length of the beam *AB*.

We introduce a fixed system of coordinate axes x_1, y_1, z_1. The system of coordinate axes x, y, z that are connected to the traverse *DE* will be movable. The origin of this system of coordinate axes will coincide with the position of the center of mass of the beam *AB* in equilibrium. Then the motion of the beam *AB* in the vertical planes xz yz will be translational and parallel to the axis x. Its movement around the axis *KC* of a bifilar fastening will be rotational and determined by the angle of rotation θ. Four coordinates x_1, x, y, θ are taken as generalized.

The axis *KC* of the bifilar fastening will perform a spherical motion around point *K* of the center of mass of the traverse. Together with the axes of the moving coordinate system, it will form auxiliary angles α, β, and γ, which are associated with generalized coordinates. When the beam *AB* rotates around the vertical axis *Cz* to an angle θ, the beam *AB* moves by an amount u along the axis *KC*. In this case, u_x, u_y, u_z it is its motion along the axes x, y, z of the moving coordinate system.

We define the kinetic and potential energies of the mechanical system as a function of the selected gene–ralized coordinates. To do this, we must calculate the coordinates of the center of mass C_θ of the beam *AB* at the current time.

Cartesian coordinates x_c and y_c the center C of the beam *AB*, which currently coincides with the point C_θ, are as follows:

$$x_\mathrm{c} = x_1 + x + u_x = x_1 + l\sin\alpha + u_x\,, \tag{1}$$

$$y_\mathrm{c} = y + u_y = l\sin\beta + u_y\,. \tag{2}$$

The vertical coordinate z_c can be found depending on the generalized coordinates x_1, x, y, θ:

$$z_\mathrm{c} = z_x + z_y + z_\theta\,,$$

where

$$\begin{aligned} z_\mathrm{x} &= l - \sqrt{l^2 - l^2\cos^2\alpha} = l - \sqrt{l^2 - x^2}\,,\\ z_\mathrm{y} &= l - \sqrt{l^2 - l^2\cos^2\beta} = l - \sqrt{l^2 - y^2}\,. \end{aligned} \tag{3}$$

The coordinate z_θ is determined by considering the bifilar fastening (fig. 2).

We denote the movement of the beam *AB* along the *KC* axis as $u = CC_\theta$.

$$AE = EA_\theta = l;\quad AC = SC = CL = a;$$
$$AL = 2a\sin\left(\theta/2\right)$$

From the triangle ESA_θ, when turning to an angle θ of the bifilar fastening, its movement u along the axis *KC* of rotation of the bifilar fastening takes the form:

$$u = l - \sqrt{l^2 - 4a^2 \sin^2(\theta/2)}\,. \tag{4}$$

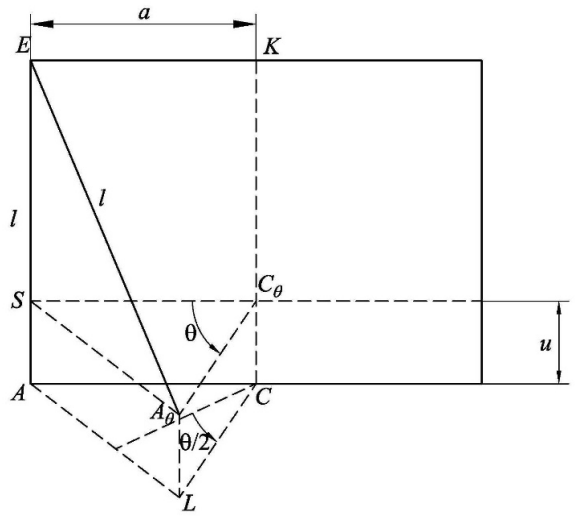

Figure 2. Computational scheme of bifilar fastening

Then the velocity of the center C of the beam AB along the axis KC of the bifilar fastening rotation at any time after simplification will be:

$$V_\theta = \frac{a^2 \cdot \sin\theta}{\sqrt{l^2 - 4a^2 \sin^2(\theta/2)}}\dot{\theta}\,. \tag{5}$$

Moving u along the axis KC of the bifilar fastening rotation with the vertical gets the angle γ. Write down the cosine value of this angle using the ratio:

$$\cos\gamma = \sqrt{1 - \sin^2\gamma} = \frac{\sqrt{l^2 - x^2 - y^2}}{l}\,. \tag{6}$$

We find the vertical coordinate z_c depending on the generalized coordinates x, y, θ (z_c it doesn't depend on the coordinate x_1):

$$\begin{aligned} z_c &= z_x + z_y + z_\theta = 2l - \sqrt{l^2 - x^2} - \sqrt{l^2 - y^2} + \\ &+ \left(1 - \sqrt{1 - 4(a/l)^2 \sin^2(\theta/2)}\right) \cdot \sqrt{l^2 - x^2 - y^2}\,. \end{aligned} \tag{7}$$

The expression for z_c is clearly non-linear.

Let us simplify expression (7) using the small para–meter method,

$$z_c = \frac{x^2}{2\ell} + \frac{y^2}{2\ell} + \frac{a^2\theta^2}{2\ell}\,. \tag{8}$$

A more extended-expression (7) for the coordinate z_c will be used for an in-depth system analysis.

Find the projections of the velocity of the center of mass of the beam AB on the axis x_1, y_1, z_1:

$$\begin{aligned} Vcx_1 &= \frac{dx_1}{dt} + \frac{dx}{dt} + V_\theta \frac{x}{l}, \\ Vcy_1 &= \frac{dy}{dt} + V_\theta \frac{y}{l}, \\ Vcz_1 &= \frac{x\dot{x}}{l} + \frac{y\dot{y}}{l} + V_\theta \frac{\sqrt{l^2 - x^2 - y^2}}{l}. \end{aligned} \tag{9}$$

4.2 The potential and kinetic energy of the mecha–nical system. Generalized forces and Lagrange equations of the second kind

The potential energy of the mechanical system (fig. 1) can be calculated as

$$\Pi = (m_2 g) \cdot z_{C_2} = m_2 g \left(\frac{x^2}{2l} + \frac{y^2}{2l} + \frac{a^2\theta^2}{2l} \right). \tag{10}$$

The potential energy (10) allows us to find the generalized forces Q_{x1}, Q_x, and Q_y which can be calculated as partial derivatives of the potential energy Π relative to the generalized coordinates x_1, x, y, θs:

$$\begin{aligned} &Q_{x1} = -\frac{\partial \Pi}{\partial x_1} \approx 0,\ Q_x = -\frac{\partial \Pi}{\partial x} \approx -m_2 g \frac{x}{l}, \\ &Q_y = -\frac{\partial \Pi}{\partial y} \approx -m_2 g \frac{y}{l},\ Q_\theta = -\frac{\partial \Pi}{\partial \theta} \approx -m_2 g \frac{a^2\theta}{l}. \end{aligned} \tag{11}$$

The vector of the generalized forces has the form:

$$\{Q\} \approx -m_2 g \cdot \frac{1}{l} \cdot \begin{pmatrix} x_1 \\ x \\ y \\ \theta \end{pmatrix}. \tag{12}$$

In this case, the kinetic energy of the mechanical system will be:

$$\begin{aligned} T = &\frac{1}{2} m_1 \left(\frac{dx_1}{dt} \right)^2 + \\ &+ \frac{1}{2} m_2 \left[\begin{aligned} &\left(\frac{dx_1}{dt} + \frac{dx}{dt} + V_\theta \frac{x}{l} \right)^2 + \left(\frac{dy}{dt} + V_\theta \frac{y}{l} \right)^2 + \\ &+ \left(\frac{x\dot{x}}{l} + \frac{y\dot{y}}{l} + V_\theta \frac{\sqrt{l^2 - x^2 - y^2}}{l} \right)^2 \end{aligned} \right] + \\ &+ \frac{1}{6} m_2 a^2 \left(\frac{d\theta}{dt} \right)^2. \end{aligned} \tag{13}$$

Simplification (13) results in the following approximate expression:

$$\begin{aligned} T = &\frac{1}{2} m_1 \left(\frac{dx_1}{dt} \right)^2 + \frac{1}{2} m_2 \left[\left(\frac{dx_1}{dt} + \frac{dx}{dt} \right)^2 + \left(\frac{dy}{dt} \right)^2 \right] + \\ &+ \frac{1}{6} m_2 a^2 \left(\frac{d\theta}{dt} \right)^2. \end{aligned} \tag{14}$$

Lagrange equations of the second kind are as follows:

$$\frac{d}{dt}\left(\frac{\partial T}{\partial \dot{q}_j} \right) - \frac{\partial T}{\partial q_j} = Q_j^a, \quad j = 1,2,3,4\,, \tag{15}$$

where $q_1 = x_1$, $q_2 = x$, $q_3 = y$, $q_4 = \theta$.

After transformations and abbreviations, we get:

$$\left(\frac{d^2 x_1}{dt^2} \right) + \frac{m_2}{m_1 + m_2} \cdot \left(\frac{d^2 x}{dt^2} \right) = 0\,, \tag{16}$$

$$\left(\frac{d^2x_1}{dt^2}+\frac{d^2x}{dt^2}\right)=-g\frac{x}{l}, \tag{17}$$

$$\left(\frac{d^2y}{dt^2}\right)=-g\frac{y}{l}, \tag{18}$$

$$\left(\frac{d^2\theta}{dt^2}\right)=-3g\frac{\theta}{l}. \tag{19}$$

Four Lagrange equations of the second kind (16)-(19) were obtained. Two of them are interconnected, and the last two are independent of each other.

Equations (16) - (19) have a solution:

$$x_1=-\frac{m_2}{m_1+m_2}\cdot x+C_1t+C_2, \tag{20}$$

$$x=A_1\sin\left(k_1t+\alpha_1\right) \tag{21}$$

$$y=A_2\sin\left(k_2t+\alpha_2\right), \tag{22}$$

$$\theta=A_3\sin\left(k_3t+\alpha_3\right). \tag{23}$$

where the integration constants depend on the initial conditions of the problem.

We can see that the laws of small relative motions of the beam in the horizontal plane have an oscillatory character with unequal frequencies:

$$k_1=\sqrt{\frac{(m_1+m_2)g}{m_2l}},\quad k_2=\sqrt{\frac{g}{l}},\quad k_3=\sqrt{\frac{3g}{l}}. \tag{24}$$

4.3 Rope tension

Using analytical geometry methods, we can find the position of the straight line *BD* in the rectangular Cartesian coordinate system x_1, y_1, and z_1. We determine the directional coefficients of the straight line *BD*:

$$\begin{gathered} m=x_B-x_D=x-a\left(l-\cos\theta\right), \\ n=y-a\sin\theta,\ p=l-z_C. \end{gathered} \tag{25}$$

To determine the tension *N* of the rope, which, due to symmetry, will be the same for each of the branches of the considered mechanical system, we can write D'Alembert's principle in the projection on the vertical axis and find:

$$N=\frac{m_2}{2}\cdot\frac{g+\ddot{z}_C}{\cos\dfrac{p}{\sqrt{m^2+n^2+p^2}}}. \tag{26}$$

5. RESEARCH RESULTS. NUMERICAL MODELING OF THE MECHANICAL SYSTEM MOTION

Using formulas (1), (2), (5), (7), (9), (11), and (13), expressions for the kinetic and potential energy take the form:

$$T=\frac{1}{2}\left(m_1V_{x1}^2+m_2\left(\begin{array}{l}\dfrac{1}{3}a^2\dot{\theta}^2+\left(\dfrac{V_{x1}+V_x+a^2x\dot{\theta}\sin[\theta]/}{\left(l\sqrt{l^2-4a^2\sin[\theta/2]^2}\right)}\right)^2+\\ +\left(V_y+a^2y\dot{\theta}\sin[\theta]\Big/\left(l\sqrt{l^2-4a^2\sin[\theta/2]^2}\right)\right)^2+\\ +\left(\dfrac{xV_x+yV_y+a^2\sqrt{l^2-x^2-y^2}\,\dot{\theta}\sin[\theta]/}{\sqrt{l^2-4a^2\sin[\theta/2]^2}}\right)^2\Big/l^2\end{array}\right)\right). \tag{27}$$

$$\Pi=gm_2(2l-\sqrt{l^2-x^2}-\sqrt{l^2-y^2}+\frac{\sqrt{l^2-x^2-y^2}\left(l-\sqrt{l^2-4a^2\sin[\theta/2]^2}\right)}{l} \tag{28}$$

Based on Lagrange equations of the second kind (15), we obtain a system of four second-order non-linear differential equations.

This system has proved to be quite cumbersome and cannot be solved analytically. Therefore, we resorted to a numerical experiment (numerical modeling) using the capabilities of computer algebra.

The following initial data and initial conditions are used for modeling: m_1=500 kg, m_2=4000 kg, l=6 m, g=9.81 m/s^2, a=2.2 m, x_{10}=0.001 m, x_0=0.5 m, y_0=0.4 m, θ_0=0.05 rad, V_{x10}=0.001 m/s, V_{x0}=0.1 m/s, V_{y0}=0.1 m/s, $\dot{\theta}_0$=0.01 rad/s.

The simulation results are shown in figures 3-11.

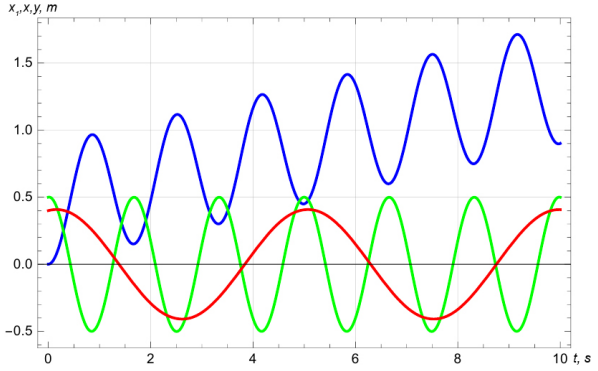

Figure 3. Graph of linear coordinates versus time: x1[t] – blue, x[t] – green, y[t] – red.

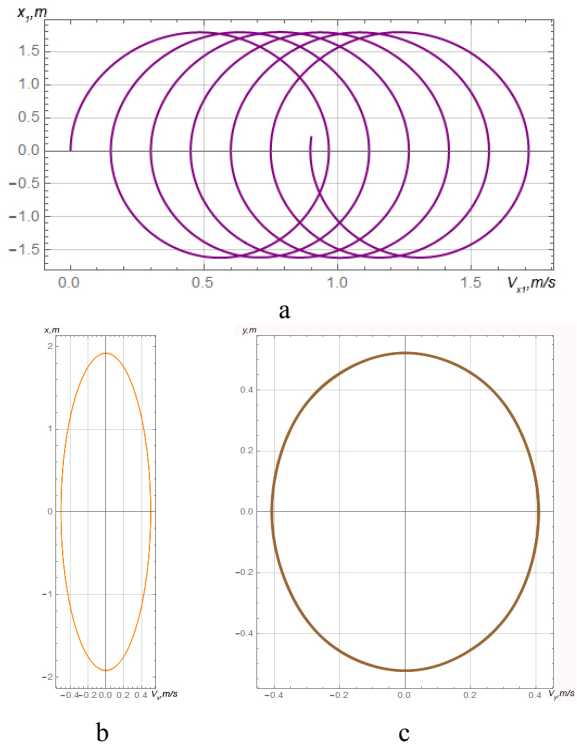

Figure 4. Phase trajectories: a – x_1-V_{x1}, b – x-Vx, c – y-V_y

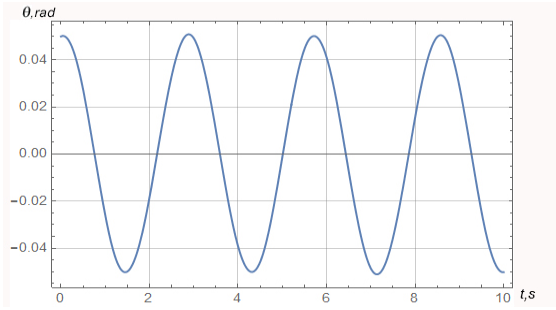

Figure 5. Dependency graph $\theta[t]$

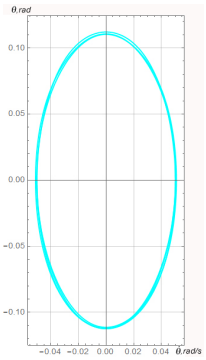

Figure 6. Phase trajectory θ-$\dot{\theta}$

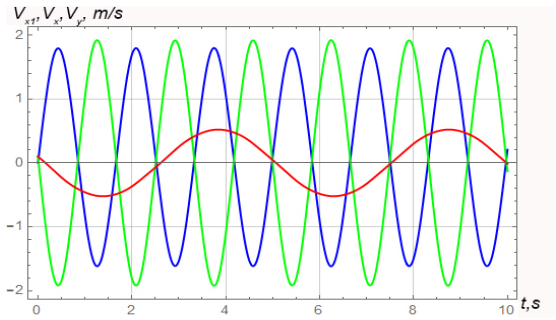

Figure 7. Graph of linear velocities versus time: $V_{x1}[t]$ – blue, $V_x[t]$ – green, $V_y[t]$ – red

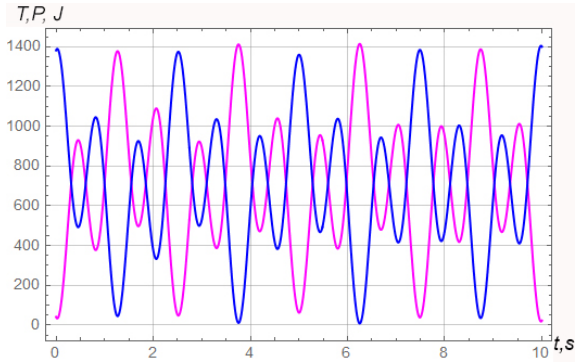

Figure 8. Graph of kinetic and potential energy versus time: $T[t]$ – purple, $P[t]$ – blue

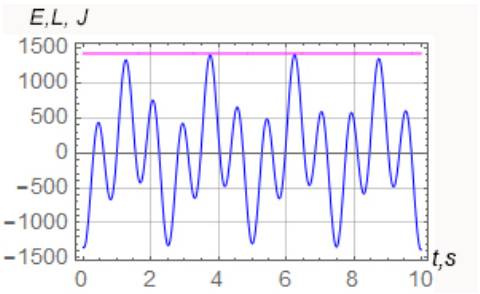

Figure 9. Graph of the total mechanical energy $E[t]$ (purple) and Lagrangian $L[t]$ (blue) versus time

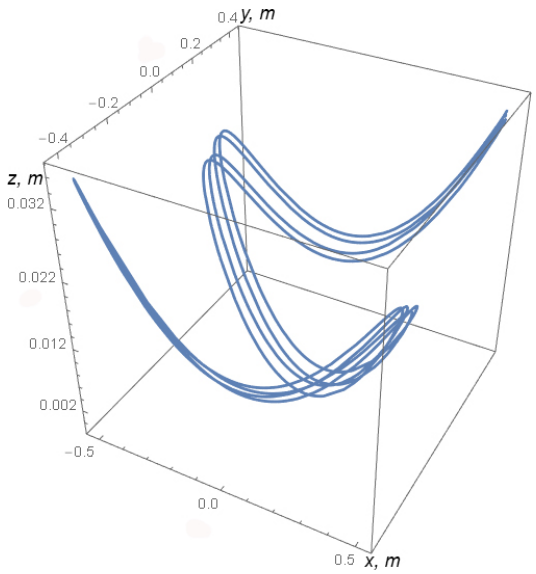

Figure 10. The spatial trajectory of the beam center of mass (point C)

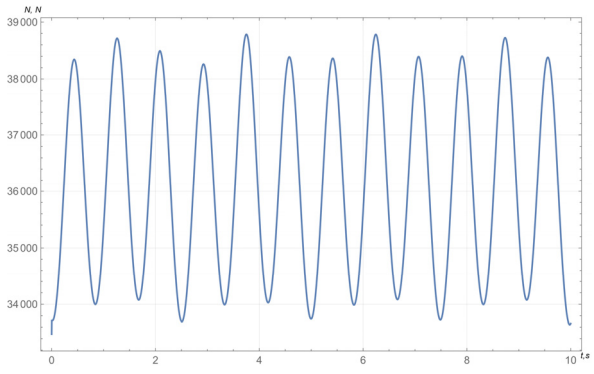

Figure 11. Graph of rope tension changes

Fig. 9 demonstrates that the graph of the total mec–hanical energy $E[t]$ is a straight horizontal line. That is,

the total mechanical energy of the system rem–ains unchanged (assuming that there are no resistance forces).

It should be noted that the presented modeling results almost coincide with the results of calculations based on simplified formulas (16)-(19).

The graph of changes in the rope tension calculated based on the (26) formula is shown in Fig. 11.

The maximum value of the rope tension was determined in the time range from 0 to 10 sec. In the indicated time range, the maximum tension is 38783.7 N, and it is reached in 3.75 sec.

6. ROPE BREAK

Let's consider the case when one of the rope branches broke when the maximum value of the rope tension was reached. For certainty, we assume that the break occurred at point *B*. We will find the tension of the second branch of the rope (branch *AE*). Let's compile the differential equations of motion of the beam *AB* for a very short period of time following the moment of break, neglecting the change in the direction of the beam and the distance of the center of mass of the beam from the other branch of the rope.

At the time of the rope breakage, the beam was in a horizontal position.

The break occurred at a certain point in time t_1, in which the beam and the trolley positions are known as x_{Ab}, x_{Eb}, y_{Ab}, y_{Eb}, z_{Cb}, x_{1b}, x_b, y_b, θ_b. We determine the directional coefficients of the line *AE* according to figure 12:

$$m_b = x_{Ab} - x_{Eb} = \left(x_{1b} + x_b - a\cos\theta_b\right) - \left(x_{1b} - a\right) = \\ = x_b + a\left(1 - \cos\theta_b\right),$$

$$n_b = y_{Ab} - y_{Eb} = y_b - a\sin\theta_b,$$

$$p_b = l - z_{Cb}.$$

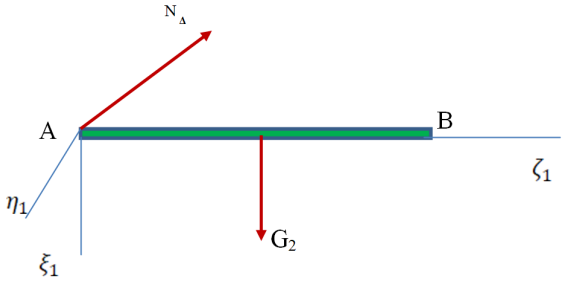

Figure 12. Calculation diagram for the rope tension N_A.

Accordingly, the angles between the line *AE* and the coordinate axes are determined by directional cosines:

$$\cos\left(\alpha_{bx}\right) = \cos\left(AE, x\right) = m_b \Big/ \sqrt{m_b^2 + n_b^2 + p_b^2},$$

$$\cos\left(\alpha_{by}\right) = \cos\left(AE, y\right) = n_b \Big/ \sqrt{m_b^2 + n_b^2 + p_b^2},$$

$$\cos\left(\alpha_{bz}\right) = \cos\left(AE, z\right) = p_b \Big/ \sqrt{m_b^2 + n_b^2 + p_b^2}.$$

For further analysis of the problem, we introduce a new coordinate system $A\zeta_1\eta_1\xi_1$, connected to the beam *AB* as shown in fig. 12. The forces acting on the beam are shown in the figure. At the same time, the directional cosines for the vector N_A of the rope *AE* tension will be:

$$\cos\left(AE, \zeta_1\right) = \cos\left(\alpha_{bx} + \theta_b\right),$$

$$\cos\left(AE, \eta_1\right) = \cos\left(\alpha_{by} + \theta_b\right),$$

$$\cos\left(AE, \xi\right) = \cos\left(\alpha\right).$$

It can be seen that the angle between the line *AE* and the vertical has not changed

Let's set up the differential equations of motion of the beam:

$$m_2 \cdot \ddot{\xi}_{1C} = G_2 - N_A \cdot \cos\left(AE, \xi_1\right), \qquad (29)$$

$$J_C \cdot \ddot{\vartheta} = N_A \cdot a \cdot \cos\left(AE, \xi_1\right), \qquad (30)$$

where $J_C = \dfrac{m_2 \cdot (2a)^2}{12} = \dfrac{m_2 \cdot a^2}{3}$ – the moment of inertia of the beam, ϑ – the angle of rotation of the beam in the vertical plane, $G_2 = m_2 g$ – the weight of the beam.

Linear and angular acceleration are related by the dependence: $\ddot{\vartheta} = \dfrac{\ddot{\xi}_{1C}}{a}$.

Then equation (30) takes the form:

$$\frac{m_2 \cdot a^2}{3} \cdot \frac{\ddot{\xi}_{1C}}{a} = N_A \cdot a \cdot \cos\left(AE, \xi_1\right),$$

here from

$$m_2 \cdot \ddot{\xi}_{1C} = 3N_A \cdot \cos\left(AE, \xi_1\right).$$

Taking into account the obtained expression, equation (29) takes the form:

$$3N_A \cdot \cos\left(AE, \xi_1\right) = G_2 - N_A \cdot \cos\left(AE, \xi_1\right).$$

Hence, we can find the tension of the rope *AE* at the moment of breaking:

$$N_A = \frac{m_2 g}{4 \cdot \cos\left(AE, \xi_1\right)} = \frac{m_2 g \sqrt{m_b^2 + n_b^2 + p_b^2}}{4 \cdot p_b}.$$

For the accepted numerical values of the initial data and initial conditions, the tension of the rope *AE* at the moment of breaking equals 9811.56 N.

7. MOVEMENT OF THE BEAM AFTER BREAKING ONE OF THE ROPE BRANCHES

From the moment of breaking of one of the rope branches, the considered mechanical system becomes a double spherical pendulum with suspension point E moving along a straight path *y* (Fig. 13).

Let's introduce a fixed (absolute or reference) coordinate system, *Oxyz*. We connect the trolley with the coordinate system $Ex_1y_1z_1$, and the beam with the coordinate systems $Ax_2y_2z_2$ and $Cx_3y_3z_3$, where p. *C* is

the center of mass of the beam AB. The system has 5 degrees of freedom. We accept $q_1 = y_1$, $q_2 = \varphi_x$, $q_3 = \varphi_y$, $q_4 = \psi_x$, $q_5 = \psi_y$ as generalized coordinates.

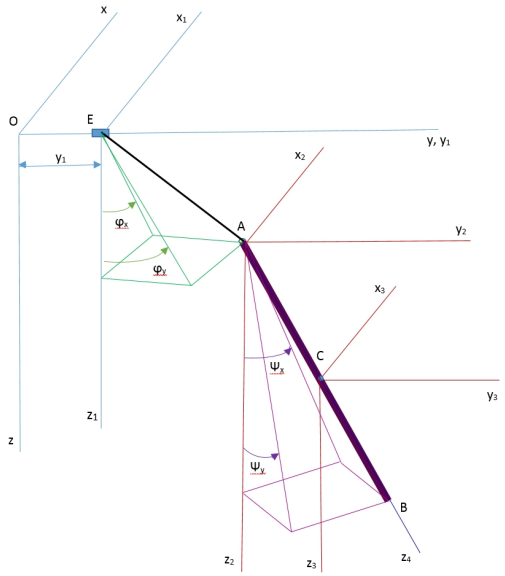

Figure 13. Calculation diagram of the beam movement after breaking one of the rope branches

The initial conditions correspond to the position of the beam AB at the moment of the rope breakage in p. B: y_{10} = -0.285m, φ_{x0} = 0.0156, φ_y = 0.36, $\psi_x = \pi/2$, $\dot{y}_{10} = 1.7\ \mathrm{m/s}$, $\dot{\varphi}_{x0} = 0$, $\dot{\varphi}_y = 0$, $\dot{\psi}_x = 0$, $\dot{\psi}_y = 0$.

The coordinate values of points A and C in the reference system $Oxyz$ are as follows:

$$x_A = l\sin(\varphi_x),$$

$$y_A = y_1 + l\cos(\varphi_x)\sin(\varphi_y),$$

$$z_A = l\cos(\varphi_x)\cos(\varphi_y),$$

$$x_C = l\sin(\varphi_x) + a\sin(\psi_x),$$

$$y_C = y_1 + l\cos(\varphi_x)\sin(\varphi_y) + a\cos(\varphi_x)\cos(\varphi_y),$$

$$z_C = l\cos(\varphi_x)\cos(\varphi_y) + a\cos(\psi_x)\cos(\psi_y).$$

The potential energy of the system:

$$P = m_2 g\begin{pmatrix} l\cdot\left(1-\cos(\varphi_x)\cos(\varphi_y)\right)+ \\ +a\left(1-\cos(\psi_x)\cos(\psi_y)\right)\end{pmatrix}$$

The kinetic energy of the system:

$$T = \frac{m_1\dot{y}_1^2}{2} + \frac{m_2 V_C^2}{2} + T_C^{(r)}, \qquad (31)$$

where $V_C^2 = \dot{x}_C^2 + \dot{y}_C^2 + \dot{z}_C^2$, $T_C^{(r)}$ is the kinetic energy of the relative motion of the beam AB in relation to its center of mass.

We draw the main central axes $Cx_4y_4z_4$ through the center of mass of point C of the beam AB so that the axis Cz_4 would pass along the axis of the beam AB, and the other two axes – perpendicularly to it. The inertia matrix of the beam relative to the main central axes has the following form:

$$J_C = \begin{vmatrix} J_1 & 0 & 0 \\ 0 & J_2 & 0 \\ 0 & 0 & J_3 \end{vmatrix} = \begin{vmatrix} \frac{m_2 a^2}{3} & 0 & 0 \\ 0 & \frac{m_2 a^2}{3} & 0 \\ 0 & 0 & 0 \end{vmatrix}. \qquad (32)$$

The transition from the coordinate system $Cx_3y_3z_3$ to $Cx_4y_4z_4$ is carried out by two consecutive rotations. The first rotation is performed around the axis Cx_3 at the angle ψ_y (Fig. 14), for which the table of the directional cosines has the form:

$$\bar{B}_1 = \begin{vmatrix} \cos(\psi_y) & 0 & \sin(\psi_y) \\ 0 & 1 & 0 \\ -\sin(\psi_y) & 0 & \cos(\psi_y) \end{vmatrix}. \qquad (33)$$

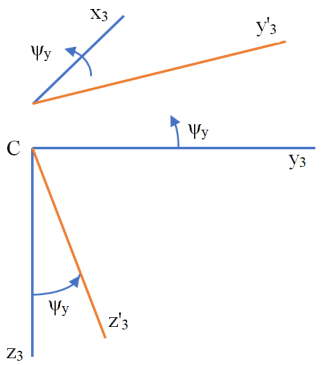

Figure 14. Scheme of the first rotation around the axis Cx_3 at the angle ψ_y

The second turn is performed around the axis Cy_3 at the angle ψ_x (Fig. 15), for which the table of the directional cosines has the form:

$$\bar{B}_2 = \begin{vmatrix} \cos(\psi_x) & -\sin(\psi_x) & 0 \\ \sin(\psi_x) & \cos(\psi_x) & 0 \\ 0 & 0 & 1 \end{vmatrix}. \qquad (34)$$

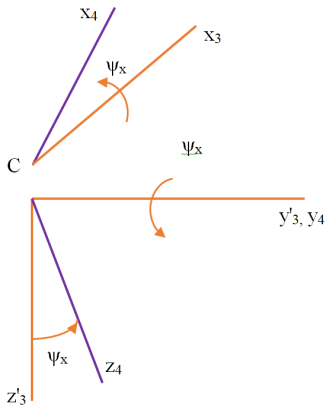

Figure 15. Scheme of the second rotation around the axis Cy_3 at the angle ψ_x

The matrix of directional cosines determines direc–tions of the main central axes:

$$\bar{B}=\bar{B}_1\cdot\bar{B}_2=\begin{vmatrix}\alpha_{11}&\alpha_{12}&\alpha_{13}\\ \alpha_{21}&\alpha_{22}&\alpha_{23}\\ \alpha_{31}&\alpha_{32}&\alpha_{33}\end{vmatrix}= \tag{35}$$

$$=\begin{vmatrix}\cos(\psi_x)\cdot\cos(\psi_y)&-\cos(\psi_y)\cdot\sin(\psi_x)&\sin(\psi_y)\\ \sin(\psi_x)&\cos(\psi_x)&0\\ -\cos(\psi_x)\cdot\sin(\psi_y)&-\sin(\psi_x)\cdot\sin(\psi_y)&\cos(\psi_y)\end{vmatrix}.$$

Moments of the inertia of the axes $Cx_3y_3z_3$:

$$\begin{aligned}J_{Cx_3}&=\alpha_{11}^2J_1+\alpha_{12}^2J_2+\alpha_{13}^2J_3=\\&=\frac{m_2a^2}{3}\left(\cos(\psi_x)\cos(\psi_y)\right)^2+\\&+\frac{m_2a^2}{3}\left(\cos(\psi_y)\sin(\psi_x)\right)^2=\\&=\frac{m_2a^2}{3}\left(\cos(\psi_y)\right)^2;\end{aligned} \tag{36}$$

$$\begin{aligned}J_{Cy_3}&=\alpha_{21}^2J_1+\alpha_{22}^2J_2+\alpha_{23}^2J_3=\\&=\frac{m_2a^2}{3}\left(\sin(\psi_x)\right)^2+\frac{m_2a^2}{3}\left(\cos(\psi_x)\right)^2=\\&=\frac{m_2a^2}{3};\end{aligned} \tag{37}$$

$$J_{Cz_3}=\alpha_{31}^2J_1+\alpha_{32}^2J_2+\alpha_{33}^2J_3=\frac{m_2a^2}{3}\left(\cos(\psi_x)\cos(\psi_y)\right)^2+ \tag{38}$$
$$+\frac{m_2a^2}{3}\left(\sin(\psi_x)\sin(\psi_y)\right)^2=\frac{m_2a^2}{3}\left(\sin(\psi_y)\right)^2;$$

The kinetic energy of the relative motion of the beam AB:

$$\begin{aligned}T_C^{(r)}&=\frac{1}{2}J_{Cx_3}\cdot\dot{\psi}_y^2+\frac{1}{2}J_{Cy_3}\cdot\dot{\psi}_x^2=\\&=\frac{m_2a^2}{6}\left(\dot{\psi}_x^2+\dot{\psi}_y^2\left(\cos(\psi_x)\right)^2\right).\end{aligned} \tag{39}$$

Lagrangian of the considered system:

$$L=T-P=\frac{m_1\dot{y}_1^2}{2}+\frac{m_2V_C^2}{2}+\frac{m_2a^2}{6}\left(\dot{\psi}_x^2+\dot{\psi}_y^2\left(\cos(\psi_x)\right)^2\right)- \tag{40}$$
$$-m_2g\begin{pmatrix}l\cdot\left(1-\cos(\varphi_x)\cos(\varphi_y)\right)+\\+a\left(1-\cos(\psi_x)\cos(\psi_y)\right)\end{pmatrix}.$$

The movement of the system is described by 5 Lagrange equations of the 2nd kind:

$$\frac{d}{dt}\left(\frac{\partial L}{\partial\dot{q}_i}\right)-\frac{\partial L}{\partial q_i}=0,\quad i=1,2,\ldots,5\,.$$

We do not present these equations in expanded form due to their cumbersomeness.

The results of the system dynamics modeling are presented below in Figures 16-19.

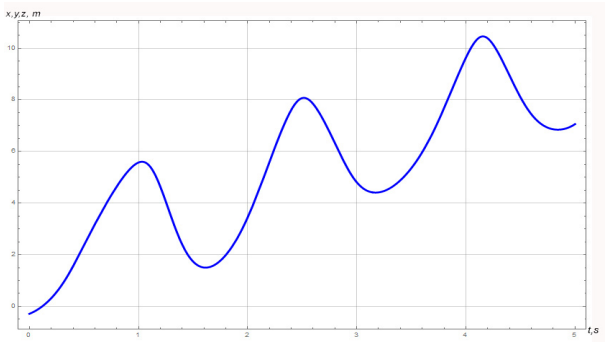

Figure 16. Dynamics of the crane trolley movement in y_1-t coordinates

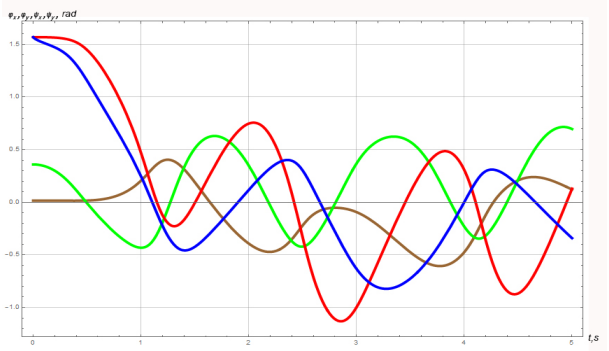

Figure 17. Graph of changes in generalized angular coordinates: φ_x – brown, φ_y – green, ψ_x – red, ψ_y – blue

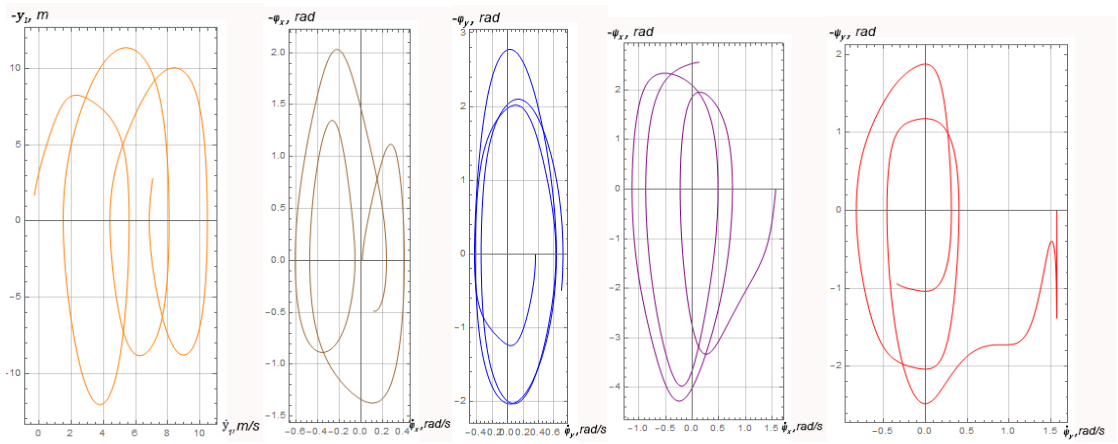

a b c d e

Figure 18. Phase trajectories: a – $y_1-\dot{y}_1$ **; b –** $\varphi_x-\dot{\varphi}_x$ **; c –** $\varphi_y-\dot{\varphi}_y$ **; d –** $\psi_x-\dot{\psi}_x$ **; e –** $\psi_y-\dot{\psi}_y$

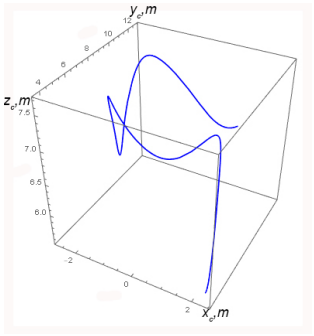

Figure 19. 3D trajectory of the center of mass of the beam (p. *C*)

Determine the rope tension in the process of moving the beam *AB*.

The differential equation of the beam motion in the projection onto the vertical axis of the fixed coordinate system:

$$m_2\ddot{z}_C = m_2 g - N\cos\varphi_x ,$$

where

$$N = m_2\frac{g-\ddot{z}_C}{\cos\varphi_x} \tag{41}$$

The schedule of changes in the rope tension over time is shown in Fig. 20. The first local extremum of the rope tension is observed at t=1.13 and is equal to 119320 N.

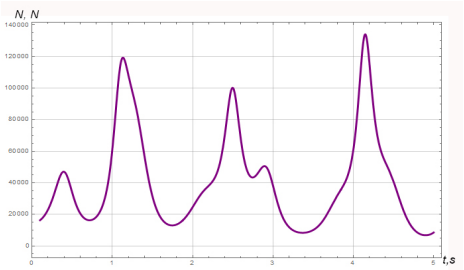

Figure 20. Graph of changing the rope tension over time

The position of the beam *AB* for the moment is determined by the coordinates: $x_C = 2.138$ m, $y_C = 5.364$ m, $z_C = 7.527$ m, $\psi_x = 0.0468$ radian, $\psi_y = -0.065$ radian. And the corresponding speeds are equal to: $V_{x_C} = -1.157$ m/s, $V_{y_C} = 2.808$ m/s, $V_{z_C} = 1.196$ m/s, $\Omega_{\psi_x} = -2.958$ radian/s, $\Omega_{\psi_y} = 2.453$ radian/s.

8. MOVEMENT OF THE BEAM AFTER THE BREAKAGE OF THE SECOND BRANCH OF THE ROPE

Suppose that at the moment of reaching the local extremum of the rope tension, it breaks, and the beam *AB* continues its free movement (Fig. 21) only under the action of gravity under the above initial conditions.

The differential equations of the beam motion will be written in the form:

$$\begin{aligned} m_2\ddot{x}_C &= 0,\\ m_2\ddot{y}_C &= 0,\\ m_2\ddot{z}_C &= m_2 g,\\ J_{Cx}\ddot{\psi}_y &= 0,\\ J_{Cy}\ddot{\psi}_x &= 0. \end{aligned} \tag{41}$$

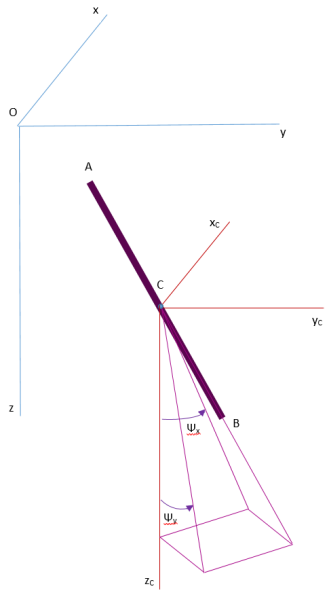

Figure 21. Scheme of free movement of the beam *AB* after the breakage of the second branch of the rope

According to formulas (36) and (37):

$$J_{Cx} = \frac{m_2 a^2}{3}\left(\cos\left(\psi_y\right)\right)^2 ;$$

$$J_{Cy} = \frac{m_2 a^2}{3} .$$

The simulation results are presented in figs. 22-24.

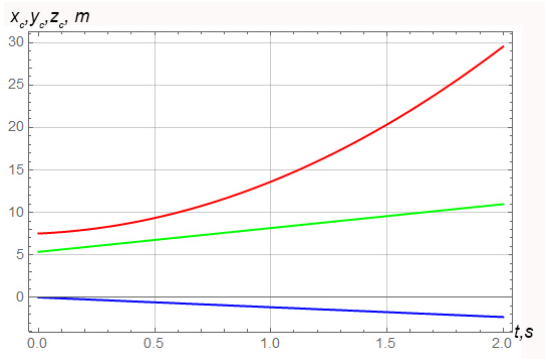

Figure 22. Movement of the center of mass of the beam: x_C – blue, y_C – green, z_C – red

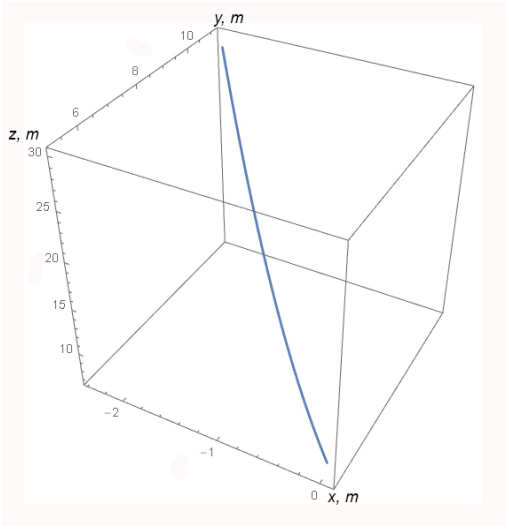

Figure 23. The 3D trajectory of the point *C*

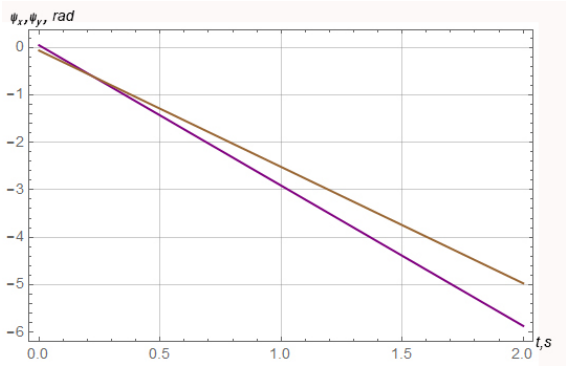

Figure 24. Changes of generalized angular coordinates: ψ_x – purple, ψ_y – brown

9. DISCUSSION OF THE RESEARCH RESULTS

The results of simulating the movement of the beam (Fig. 3) with the specified numerical values of the system parameters show that the trolley moves along the guides, moving away from the initial position and making oscillations with an amplitude of approximately 0.5 m in a period of 5 sec during the considered time interval of 10 sec. At the same time, the trolley moves at a distance of 0.9 m. The range of oscillations of the center of mass of the beam along the x and y coordinate axes is 0.9 and 0.8 m, respectively. At the same time, the period of oscillations along the axis x is equal to approximately 1.7 sec. It is less than the period of oscillations along the axis y by approximately 3 times.

Since the problem was solved without taking into account the resistance forces, the phase trajectories in Fig. 4 came out in the form of ellipses.

The graph of changes in time and the phase trajectory of the angle θ demonstrate the harmonic nature of oscillations with an amplitude of 0.046 rad/s and a period of approximately 0.95 s.

Figure 8 demonstrates the implementation of the law of mechanical energy conservation. It can be seen that the kinetic and potential energies of the system are in antiphase, and the total mechanical energy of the system does not change (see Fig. 9).

The trajectory of the center of mass of the beam is shown in three-dimensional Cartesian space (Fig. 10), which indicates the complex nature of this movement.

The calculation performed in paragraph 7 shows that the tension of the intact branch of the rope at the time of the breakage of the second branch is significantly less than the amount of tension of the rope before the break.

After one branch of the rope breaks, the trolley moves away from the position it occupied at the time of the breakage. At the same time, the trolley demonstrates an uneven oscillating motion.

Figs. 16 and 18a demonstrate the law of the conservation of momentum of the mechanical system.

As can be seen from Figures 17 and 18b,c,d,e, the generalized coordinates φx, φy perform oscillatory movements near zero. And the generalized coordinates ψx, ψy start to move from the value π/2 and tend to zero during the movement.

3D-trajectory of the point *C* of the center of mass of the beam within the considered time interval (Fig. 19) shows that the beam tends to move from a horizontal to a vertical position.

Calculation of the rope tension over time (Fig. 20) shows significant dynamic loads. The tension can be approximately three times greater than the weight of the beam itself. This can lead to the break of the second branch of the rope.

And after the break of the second branch of the rope, the beam moves under gravity only as a free solid body with a distributed mass. According to the laws of classical mechanics, the horizontal coordinates of the center of mass of the beam and the angular coordinates change linearly, but the vertical coordinate changes along a parabola.

In addition, the study of the characteristic move–ments of the load and the nature of the oscillations provide the basis for choosing the optimal method (controlled movements of the crane, use of dampers, etc.) and equipment to eliminate the negative conse–quences or reduce their impact. This should signi–ficantly increase the productivity of the use of crane equipment and its reliability (to increase the speed of carrying out cargo operations, eliminate oscillations in the system to increase the durability of the equipment, and reduce the probability of emergencies).

10. CONCLUSION

1. The complex problem of moving a body with a distributed mass (a beam), which includes three stages, is considered. In the first stage, the movement of the beam suspended to a mobile trolley by a bifilar fas–tening is investigated. The second stage begins at the moment of the breakage of one of the two ropes, and then the movement of the mechanical system "trolley-rope-beam" is simulated. It is assumed that the rope breaks at the time of reaching a maximum value of its tension, and, in the third stage, movement of the beam only is considered. All stages are connected by the fact that the final values of the motion parameters at the previous stage (coordinates and velocities) are the initial parameters for studying the motion of the mechanical system at the next stage.

2. 4 DOF mechanical system "movable trolley with the beam" is studied. Using Lagrange equations, a sys–tem of four non-linear differential equations of the second order is obtained, which describes the motion of the considered mechanical system. Depending on the four generalized coordinates, expressions for the kinetic and potential energies are defined for compiling the equations of motion. The resulting system of equations is solved numerically using computer algebra.

3. The proposed system of Lagrange equations of the second order for a 4 DOF mechanical system with the assumption of small oscillations is also solved analy–tically. The results of the analytical and the numerical solutions almost coincide.

4. The system movement's peculiarities and charac–teristics - two interdependent horizontal rectilinear mo–vements and independent lateral movement - are deter–

mined. The problem of a bifilar fastening of the beam is solved by studying the vertical movement. Three inde–pendent oscillations and their frequencies are found. The conservatism of the mechanical system is empha–sized.

5. With the help of the D'alambert principle, the mag–nitude of the rope tension and its extreme values are determined.

6. For the case when one of the branches of the ropes cannot withstand the load and the beam continues to move on the second one, the magnitude of tension of the remaining rope branch is found at the moment of the breakage of the first branch. The mechanical system is a double spherical pendulum with a suspension point moving along a rectilinear horizontal trajectory. 5 DOF differential equations of the beam motion were set up and the results of numerical simulation of a new mechanical system were obtained. The values of the coordinates and their derivatives at the time of the break of the rope branch are used as the initial conditions of the simulation. The change in the rope tension over time is calculated, and its extreme values are determined.

7. A mathematical model is developed, and the beam motion after the breakage of the second branch of the rope at the moment of reaching the maximum tension is investigated. The beam motion is performed according to the laws of free fall in space and is described by the 5 DOF system of differential equations for which numerical simulation is also performed.

8. Simulation of emergencies related to rope breakage can become a basis for preventing their occurrence and minimizing negative consequences.

9. The study of characteristic movements of the load and the nature of the oscillations provides the basis for choosing the best way to eliminate them or reduce their impact (crane-controlled movements, dampers, etc.). This should make it possible to significantly increase the productivity of the used crane equipment (it allows to an increase in the speed of carrying out cargo operations) and its reliability (the elimination of oscillations in the system increases the durability of the equipment and reduces the probability of emergencies).

10. The obtained results will be used for further study of the system to reduce the rope tension and the amplitude of the beam oscillations by using the method of controlled crane movement.

11. Consideration of damping and elastic properties of the system will be the subject of further research.

REFERENCES

[1] Loveikin, V., Romasevych, Y., Shymko, L., Ohiienko, M., Duczmal, W., Potwora, W. et al. (2020). Agrotronics and optimal control of cranes and hoisting machines: monograph. Poland, Opole: The Academy of Management and Administration in Opole.

[2] Kenan H., & Azeloğlu, O. (2020). Design of scaled down model of a tower crane mast by using similitude theory. Engineering Structures, 220:110985. doi:10.1016/j.engstruct.2020.110985.

[3] Tian, J., Luo, S., Wang, X., Hu, J., & Yin, J. (2021). Crane Lifting Optimization and Construction Monitoring in Steel Bridge Construction Project Based on BIM and UAV. Hindawi, Advances in Civil Engineering. Volume 2021, Article ID 5512229, 15 pages. doi:10.1155/2021/5512229.

[4] Hong, K.-S., & Shah U.H. (2019). Dynamics and Control of Industrial Cranes. Monograph. Advances in Industrial Control. Singapore: Springer. doi:10.1007/978-981-13-5770-1.

[5] Luigi Solazzi, L. (2020). Effect of Recurrent Impulse Load Actions on a Crane. FME Transactions, Vol. 48, No. 2, pp. 266-271, doi: 10.5937/fme2002266S.

[6] Stölzner, Manuel & Kleeberger, Michael & Günthner, Willibald & Fottner, Johannes. (2020). Calculating the dynamic behaviour of lattice boom mobile cranes during hoisting, FME Transactions. Vol. 48. pp. 313-318. Doi: 10.5937/fme2002313S.

[7] Aguiar, C., Leite, D., Pereira, D., Andonovski, G., & Škrjanc, I. (2021). Non-linear modeling and robust LMI fuzzy control of overhead crane systems. Journal of the Franklin Institute, vol. 358, pp. 1376–1402.

[8] Litak, G., Margielewicz, J., Gaska, D., Yurchenko, D., & Dabek, K. (2020). Dynamic response of the spherical pendulum subjected to horizontal Lissajous excitation. Nonlinear Dyn 102, 2125–2142. doi:10.1007/s11071-020-06023-5.

[9] Solazzi, L., & Zrnić, N. (2020). Dynamic Analyses of Gantry Crane Under Several Trolley and Payload Movements, FME Transactions, Vol. 48, No. 2,pp. 281-286, doi:10.5937/fme2002281S

[10] Nguyen, T. K. (2021). Combination of feedback control and spring-damper to reduce the vibration of crane payload. Archive of mechanical engi–neering. Volume 68 number 2. doi:10.24425/ame. 2021.137046.

[11] Shao, X., Zhang, J., Zhang, X., Zhao, Z., & Chen Z. (2019). A novel anti-swing and position control method for overhead crane. Science Progress, 103(6), 1–24. doi:10.1177/0036850419883539.

[12] Fatehi, M.H., Eghtesad, M., Necsulescu, D.S., & Fatehi, A.A. (2019). Tracking control design for a multi-degree underactuated flexible-rope overhead crane system with large swing angle based on singular perturbation method and an energy-shaping technique. Journal of Vibration and Control, 25(11), 1752-1767. doi:10.1177/10775 46319833881.

[13] Liu, H., Cheng, W., & Li, Y. (2019). Dynamic Responses of an Overhead Crane's Beam Sub–jected to a Moving Trolley with a Pendulum Pay–load. Shock and Vibration. Volume 2019. Article ID 1291652. 14 pages. doi:10.1155/2019/1291652.

[14] Zrnic, Nenad & Petković, Zoran & Bošnjak, Srđan. (2005). Automation of ship-to-shore

container cranes: A review of state-of-the-art. FME Transactions, Vol. 33, pp. 111-121.
[15] Bugaric, Ugljesa & U., Vuković. (2002). Optimal control of motion of the system based on mathematical pendulum with constant length. FME Transactions, Vol. 30.
[16] Singhose, W.E. & Jason, Lawrence & Sorensen, Khalid & Kim, Dooroo. (2006). Applications and educational uses of crane oscillation control, FME Transactions, Vol. 34.
[17] Shi, H., Li, G, Ma, X., & Sun, J. (2019). Research on Non-linear Coupling Anti-Swing Control Method of Double Pendulum Gantry Crane Based on Improved Energy. Symmetry, 11, 1511; 20 p. doi:10.3390/sym11121511.
[18] Chai, L., Guo, Q., Liu, H., & Ding, M. (2021). Linear Active Disturbance Rejection Control for Double-Pendulum Overhead Cranes. IEEE Access, Volume 9. doi:10.1109/ACCESS.2021.3070048.
[19] Hai-yan Qiang, You-gang Sun, Jin-chao Lyu, & Da-shan Dong. (2021). Anti-Sway and Positioning Adaptive Control of a Double-Pendulum Effect Crane System With Neural Network Compensation. Journal List Front Robot AI v.8. doi:10.3389/frobt.2021.639734.
[20] Jaafar, H.I., Mohamed, Z., Shamsudin, M.A., Mohd Subha, N.A., Liyana Ramli, L., & Abdu–llahi, A.M. (2019). Model reference command shaping for vibration control of multimode flexible systems with application to a double-pendulum overhead crane. Mechanical Systems and Signal Processing 115, 677–695. doi:10.1016/j.ymssp. 2018.06.005.
[21] Perig, A.V., Stadnik, A.N., Deriglazov, A.I., & Podlesny S.V. (2014) 3 DOF spherical pendulum oscillations with a uniform slewing pivot center and a small angle assumption. Shock and Vibration. Vol. 2014. Article ID 203709. 32 p. doi:10.1155/2014/203709.
[22] Jeloka, B. (2021). Almost Globally Asymptotically Stable Switched PD Control for a Spherical Pendulum. 29th Mediterranean Conference on Control and Automation (MED), Vol. 00, 1258-1263 doi:10.1109/med51440.2021.9480292.
[23] Freundlich, J., & Sado, D. (2020). Dynamics of a coupled mechanical system containing a spherical pendulum and a fractional damper. Meccanica, 55 (3). doi:10.1007/s11012-020-01203-4.
[24] Podlesny, S. (2020) Dynamics of a spherical pendulum on a non-linear elastic suspension under the action of a variable side aerodynamic load. Visnyk TNTU, Vol 98, No2, 49–58. doi:10.33108 /visnyk_tntu2020.02.049.
[25] Cekus, D., & Kwiatoń, P. (2020). Effect of the rope system deformation on the working cycle of the mobile crane during interaction of wind pressure. Mechanism and Machine Theory, 153, 104011 doi:10.1016/j.mechmachtheory.2020.104011.
[26] Liu, Z., Sun, N., Wu, Y., Xin, X., & Fang, Y. (2021). Non-linear Sliding Mode Tracking Control of Underactuated Tower Cranes. International Journal of Control Automation and Systems 19(11), 1065-1077. doi:10.1007/s12555-020-0033-5.
[27] Shi, H., Li, G., Bai, X., & Huang, J. (2019). Research on Nonlinear Contro l Method of Underactuated Gantry Crane Based on Machine Vision Positioning. Symmetry, 11, 987. doi:10.3390/sym11080987.
[28] Maghsoudi, M.J., Nacer, H., Tokhi, M.O., & Mohamed Z. (2018). A Novel Approach in S-Shaped Input Design for Higher Vibration Reduction. Journal of Applications of Modelling and Simulation, 2(2), 76-83.
[29] Kostikov, A., Perig, A., Larichkin, O., Stadnik, A., & Gribkov, E (2019). Research into payload swaying reduction through rope length manipulation during Boom crane motion, FME Transactions, Vol. 47, No. 3, pp. 464-476, doi: 10.5937/fmet1903464K.
[30] Fasih, S.M., Mohamed, Z., Husain, A.R., Ramli, L., Abdullahi, A.M., & Anjum, W. (2020). Payload swing control of a tower crane using a neural network–based input shaper. Measurement and Control. Vol. 53(7-8), 1171–1182. doi:10.1177/0020294020920895.
[31] Loveikin, V., Romasevych, Y., Kadykalo, I., & Liashko, A. (2019). Optimization of the swinging mode of the boom crane upon a complex integral criterion. Journal of Theoretical and Applied Mechanics, Vol.49, 285-296. doi:10.7546/JTAM.49.19.03.07.
[32] Boskovic, Goran & Markovic, Goran & Savković, Mile & Zdravković, Nebojša. (2016). Review of the dynamic and mathematical models of portal slewing cranes. IMK-14 - Istrazivanje i razvoj. 22. 113-118. 10.5937/IMK1604113B.
[33] Sawodny, Oliver & Neupert, Jörg & Arnold, Eckhard. (2009). Actual trends in crane automation: Directions for the future, FME Transactions, Vol. 37, pp. 167-174.
[34] Wang, R., Chen, Z., Zhang, W., & Zhu, Q. (Eds.) (2019). Proceedings of the 11th International Conference on Modelling, Identification and Control (ICMIC2019), Lecture Notes in Electrical Engineering 582, 215-226.
[35] Abdullahi, A.M., Mohamed, Z., Selamat, H., Pota, H.R., Zainal Abidin, M.S., & Fasih, S.M. (2020). Efficient control of a 3D overhead crane with simultaneous payload hoisting and wind disturbance: design, simulation and experiment. Mechanical Systems and Signal Processing, Vol. 145, 106893, 16 p. doi:10.1016/j.ymssp.2020.106893.
[36] Ambrosino, M., Berneman, M., Carbone, G., Crépin, R., Dawans, A., & Garone, E. (2020). Modeling and Control of 5-DoF Boom Crane. 2020 Proceedings of the 37th ISARC, Kitakyushu, Japan, 514-521. doi:10.22260/ISARC2020/0071.
[37] Yang, T., Sun, N., Chen, H., & Fang, Y. (2020). Swing suppression and accurate positioning control for underactuated offshore crane systems suffering from disturbances. IEEE/CAA JOURNAL OF AUTOMATICA SINICA, VOL. 7 (3), 892-900.

[38] Cao, Y., & Li, T. (2020). Review of antiswing control of shipboard cranes. IEEE/CAA JOURNAL OF AUTOMATICA SINICA, VOL. 7(2), 346-354. doi:10.1109/JAS.2020.1003024.
[39] Perig, A. V., Stadnik, A.N., Kostikov, A.A., & Podlesny, S.V. (2017) Research into 2D dynamics and control of small oscillations of a cross-beam during transportation by two overhead cranes. Shock and Vibration, Volume 2017, 9605657. doi:10.1155/2017/9605657.
[40] Wu, Q., Wang, X., Hua, L., & Xia, M. (2021). Modeling and non-linear sliding mode controls of double pendulum cranes considering distributed mass beams, varying roped length and external disturbances. Mechanical Systems and Signal Processing, 158, 107756. doi: 10.1016/j.ymssp, 2021. 107756.
[41] Singhose, W.E. & Peng, K. & Garcia, A. & Ferri, Aldo. (2016). Modeling and control of crane payload lift-off and lay-down operations. FME Transactions, Vol. 44, pp. 237-248, doi: 10.5937/fmet1603237S.
[42] Sun, N., Fu, Y., Yang, T., Zhang, J., Fang, Y., & Xin, X. (2020). Non-linear Motion Control of Complicated Dual Rotary Crane Systems Without Velocity Feedback: Design, Analysis, and Hardware Experiments. IEEE Transactions On Automation Science And Engineering, 2020. doi:10.1109/TASE.2019.2961258.
[43] Ye, J., & Huang, J. (2021). Analytical Analysis and Oscillation Control of Payload Twisting Dynamics in a Tower Crane Carrying a Slender Payload. Mechanical Systems and Signal Processing, September 2021. doi:10.1016/j.ymssp. 2021.107763.
[44] Huang, J, & Zhu, K, (2020). Dynamics and control of three-dimensional dual cranes transporting a bulky payload. Proceedings of the Institution of Mechanical Engineers, Part C: Journal of Mechanical Engineering Science. doi:10.1177/0954406220949579.
[45] Yao, X., Feng, Y., Meng, L., Yao, L., & Li, H. (2021). Influence of structural elasticity on transshipment dynamics of dual-trolley overhead crane. Advances in Mechanical Engineering, Vol. 13(7) 1–21. doi:10.1177/16878140211031029.

ПРОСТОРНИ ТРАНСПОРТ ГРЕДЕ ПРИ БИФИЛАРНОМ ПРИЧВРШЋИВАЊУ

А. Стадник, С. Подлесни, С. Капорович, А. Кабатски

Истражује се сложен проблем просторног кретања механичког система „колица-греда”. Разматрају се три стадијума: 1) кретање греде на бифиларној суспензији до покретних колица; 2) кретање греде након лома једне гране суспензије; 3) кретање греде након лома друге гране суспензије. Студија је спроведена креирањем математичких модела за сваку фазу кретања система, а затим извођењем нумеричког експеримента коришћењем компју–терске алгебре. Напетост ужади се израчунава у првој и другој фази кретања система. Њихове екстремне вредности су одређене. Добијени резултати ће се користити у даљем проучавању система за смањење затезања ужета и амплитуде осциловања и за спречавање незгода.